

引用格式：霍海龙，陈正乐，张青，等，2024. 新疆西昆仑 509 道班西锂矿伟晶岩石英变形特征、温度及其对伟晶岩就位的约束 [J]. 地质力学学报, 30 (1) : 72–87. DOI: [10.12090/j.issn.1006-6616.2023078](https://doi.org/10.12090/j.issn.1006-6616.2023078)

Citation: HOU H L, CHEN Z L, ZHANG Q, et al., 2024. Quartz deformation characteristics, deformation temperature, and their constraints on pegmatites of the 509 Daobanxi lithium deposit in the West Kunlun area, Xinjiang[J]. Journal of Geomechanics, 30 (1) : 72–87. DOI: [10.12090/j.issn.1006-6616.2023078](https://doi.org/10.12090/j.issn.1006-6616.2023078)

## 新疆西昆仑 509 道班西锂矿伟晶岩石英变形特征、温度及其对伟晶岩就位的约束

霍海龙<sup>1,2</sup>, 陈正乐<sup>1,2,3,4</sup>, 张青<sup>1,2</sup>, 王永<sup>1,2</sup>, 马华东<sup>4,5</sup>, 王威<sup>3,4</sup>, 张文高<sup>1,2,3</sup>,  
李永<sup>6</sup>, 韩凤彬<sup>1,2</sup>, 杜晓飞<sup>4,5</sup>, 闵壮<sup>1</sup>, 孟祥鹏<sup>1</sup>

HOU Hailong<sup>1,2</sup>, CHEN Zhengle<sup>1,2,3,4</sup>, ZHANG Qing<sup>1,2</sup>, WANG Yong<sup>1,2</sup>, MA Huadong<sup>4,5</sup>, WANG Wei<sup>3,4</sup>,  
ZHANG Wengao<sup>1,2,3</sup>, LI Yong<sup>6</sup>, HAN Fengbin<sup>1,2</sup>, DU Xiaofei<sup>4,5</sup>, MIN Zhuang<sup>1</sup>, MENG Xiangpeng<sup>1</sup>

1. 中国地质科学院地质力学研究所, 北京 100081;
  2. 自然资源部古地磁与古构造重建重点实验室, 北京 100081;
  3. 自然资源部深地科学与探测技术实验室, 北京 100094;
  4. 新疆自然资源与生态环境研究中心, 新疆 乌鲁木齐 830000;
  5. 新疆维吾尔自治区人民政府国家 305 项目办公室, 新疆 乌鲁木齐 830000;
  6. 新疆维吾尔自治区有色地质勘查局地质矿产勘查研究院, 新疆 乌鲁木齐 830099
1. *Institute of Geomechanics, Chinese Academy of Geological Sciences, Beijing 100081, China*;
  2. *Key Laboratory of Paleomagnetism and Tectonic Reconstruction of Ministry of Natural Resources, Beijing 100081, China*;
  3. *SinoProbe Laboratory, Chinese Academy of Geological Sciences, Beijing 100094, China*;
  4. *Research Center Resource and Environment of Xinjiang Uygur Autonomous Region, Urumqi 830000, Xinjiang, China*;
  5. *National 305 Project Office of Xinjiang Uygur Autonomous Region, Urumqi 830000, Xinjiang, China*;
  6. *Institute of Geology and Mineral Resources Exploration, Nonferrous Geological Exploration Bureau of Xinjiang Uygur Autonomous Region, Urumqi 830099, Xinjiang, China*

## Quartz deformation characteristics, deformation temperature, and their constraints on pegmatites of the 509 Daobanxi lithium deposit in the West Kunlun area, Xinjiang

**Abstract:** [Objective] The 509 Daobanxi deposit in the West Kunlun orogenic belt is a newly discovered large pegmatite-type lithium-polymetallic deposit in northwestern China. As a typical granite pegmatite lithium deposit in the region, the metallogenetic characteristics and pegmatite evolution of the 509 Daobanxi deposits are of great significance for understanding the entire lithium-polymetallic mineralization process of the West Kunlun metallogenic belt. The granite pegmatites contain assemblages of plagioclase, spodumene, quartz, muscovite, etc., exhibiting strong mylonization and

基金项目：国家自然科学基金项目(42172258, 42072227); 国家重点研发计划项目(2021YFC2901904, 2021YFC2901805); 新疆维吾尔自治区重大专项项目(2023A03002); 中国铀业有限公司-东华理工大学核资源与环境国家重点实验室联合创新基金项目(NRE2021-01); 中国地质调查局地质调查项目(DD20221660-3, DZLXJK202206)

This research is financially supported by the National Natural Science Foundation of China (Grants No. 42172258 and 42072227), the National Key Technology Research and Development Program of the Ministry of Science and Technology of China (Grants No. 2021YFC2901904 and 2021YFC2901805), the Science and Technology Major Project of Xinjiang Uygur Autonomous Region, China (Grant No. 2023A03002), the Joint Innovation Fund of China National Uranium Co., Ltd and State Key Laboratory of Nuclear Resources and Environment (Grant No. NRE2021-01), and the Projects of China Geological Survey (Grants No. DD20221660-3 and DZLXJK202206).

第一作者：霍海龙（1988—），男，博士，助理研究员，主要从事矿田构造研究工作。Email: [huohailong2012@163.com](mailto:huohailong2012@163.com)

通讯作者：陈正乐（1967—），男，博士，研究员，主要从事矿田构造研究工作。Email: [chenzhengle@263.net](mailto:chenzhengle@263.net)

收稿日期：2023-05-18；修回日期：2023-12-05；录用日期：2024-01-03；网络出版日期：2024-01-15；责任编辑：范二平

forming typical ductile deformation characteristics in the 509 Daobanxi deposit. Quartz, an essential mineral in granite pegmatite, is ideal for tracking pegmatite's mineralization process and studying the deformation behavior of continental rocks in long-term geological history. [Methods] To study the late-stage emplacement process of pegmatite evolution, comprehensive analyses were conducted on the quartz deformation structures measurements, fluid inclusion temperature, and quartz trace elements for the 509 Daobanxi granite pegmatites. Cathodoluminescence (CL) analysis of quartz in deformed granite pegmatite samples was performed to reveal the compositional zoning of Ti in quartz. Laser ablation inductively coupled plasma mass spectrometry (LA-ICP-MS) was used to analyze 64 points from samples Zk2707-9 and Zk1107-2. [Results] The minerals of spodumene and plagioclase in deformed pegmatites primarily show brittle fracturing characteristics, with the features of rigid body deformation and the muscovite presence of mica-fish. Meanwhile, the conspicuous feature is that quartz grains mainly develop dynamic recrystallization and contain subgrains. According to the microstructural characteristics of spodumene, plagioclase, and quartz, the deformation temperature of mylonitized granite pegmatite is 300~400°C. The CL images of quartz bands in the granite pegmatite samples have no apparent zoning, indicating that the Ti content reaches a relative equilibrium state in the quartz deformation stage. The LA-ICP-MS analysis shows quartz from the 509 Daobanxi granite pegmatites contains a lower concentration of Ti ( $1.03 \times 10^{-6}$  to  $7.67 \times 10^{-6}$  and  $1.04 \times 10^{-6}$  to  $6.75 \times 10^{-6}$ ), suggesting relatively lower deformation temperatures. The Ti-in-quartz thermobarometry indicates quartz deformation temperatures ranging from 371 to 398°C and 351 to 377°C, respectively. The thermometric measurement shows that homogenization temperatures of the quartz fluid inclusions in pegmatite varied from 260°C to 283°C, likely recording the temperature of the late stage of pegmatite evolution. [Conclusion] Comprehensive analysis shows that the 509 Daobanxi granite pegmatites underwent a period of intense ductile deformation during the emplacement process, with low temperature and high strain rate. The emplacement of pegmatite is a product of the rapid cooling process, and the grain size reduction caused by dynamic recrystallization (GBM) under high-stress and low-temperature conditions profoundly changed the rheological properties of pegmatite. The supercooling process from ~400°C to ~260°C ( $\Delta T=140^{\circ}\text{C} \pm$ ), resulting in less rapid mineral crystalline new nuclei in pegmatites, is more conducive to the formation of coarse quartz and other mineral particles, forming the significant characteristics of granite pegmatites. [Significance] In fact, the emplacement process of granitic pegmatites remains a puzzle, and high-quality, accurate systematic work is needed to understand the evolution process and behavior of granite pegmatite. By studying the 509 Daobanxi granite pegmatites, we proposed that the pegmatite emplacement was a product of the rapid cooling process, and supercooling plays an essential role in pegmatite emplacement. Similar deformation characteristics are widely developed in the Tugeman lithium deposit in the Altyn Tagh area and the Jiajika lithium deposit in the western Sichuan. Although the current work is preliminary, our study provides some clues for exploring the emplacement process of granitic pegmatites.

**Keywords:** mylonization; lithium ore; granite pegmatites; 509 Daobanxi area; West Kunlun; Xinjiang

**摘要:** 509道班西锂矿床是西昆仑造山带新近发现的大型伟晶岩型锂多金属矿床。作为区内典型的花岗伟晶岩型锂矿床, 509道班西锂矿的成矿机制和伟晶岩演化过程对认识整个西昆仑成矿带的成矿作用具有重要意义。作为花岗伟晶岩中的重要矿物, 石英是追踪伟晶岩成矿作用过程的理想对象。509道班西矿床的花岗伟晶岩普遍发育强烈的糜棱岩化作用, 具有典型的韧性变形特征, 通过对糜棱岩化伟晶岩脉进行变形组构分析、石英包裹体测温和石英Ti温度计计算, 揭示了与伟晶岩就位相关的大陆地壳变形过程中流体的热力学演化过程, 并探讨了韧性变形对区域找矿的启示意义。糜棱岩化伟晶岩中锂辉石、斜长石等矿物主要以脆性破裂为主, 具有刚体变形的特征; 石英主要发育膨凸重结晶现象, 细小的新晶体在较大的石英条带边部形成, 可见石英残斑, 并具有亚颗粒旋转现象, 部分发育核幔构造; 白云母普遍变形成云母鱼。石英包裹体、锂辉石和石英的变形特征等微观结构证据表明, 糜棱岩化伟晶岩的变形温度为300~400°C, 石英Ti温度计得出的变形温度为371~398°C和351~377°C。伟晶岩中石英包裹体的均一温度平均为260~283°C, 可能记录了石英变形晚阶段的温度。研究表明, 509道班西地区的伟晶岩在侵位过程中经历了一期强烈的低温、高应变速率的韧性变形, 伟晶岩就位是快速冷却过程的产物, 在高应力和较低温度条件下, 动态重结晶(GBM)导致的晶粒粒径减小严重改变了岩石的流变学性质; 从~400°C到~260°C的超冷却过程( $\Delta T=\pm 140^{\circ}\text{C}$ )中, 造成伟晶岩中矿物结晶新核迅速减少, 更有利于形成粗大的石英等矿物颗粒, 形成伟晶岩脉所有显著特征和独特的岩石结构和矿物组合的空间分带, 超冷却在伟晶

岩就位过程中具有重要的作用。

**关键词:** 糜棱岩化; 锂矿床; 花岗伟晶岩; 509道班西地区; 西昆仑; 新疆

**中图分类号:** P613; P548      **文献标识码:** A      **文章编号:** 1006-6616 (2024) 01-0072-16

DOI: [10.12090/j.issn.1006-6616.2023078](https://doi.org/10.12090/j.issn.1006-6616.2023078)

## 0 引言

锂(Li)作为重要的稀有金属元素之一,对国家经济和国防安全至关重要,目前对于锂元素的超常富集机制认识较浅,严重制约着其资源的预测评价(Xu et al., 2021; 郑范博等, 2021; 唐文春等, 2022; 王登红等, 2022; 李建康等, 2023; 王核等, 2023)。随着大红柳滩锂矿、白龙山锂矿、509道班西锂矿和雪凤岭锂矿等一系列锂(铍)矿床的发现,形成了西昆仑大红柳滩-白龙山巨型伟晶岩型锂多金属成矿带(王核等, 2017, 2021; Wang et al., 2020; 陈谋等, 2022; 李永等, 2022; 王威等, 2022)。作为大红柳滩地区典型的锂多金属矿床,相关学者对509道班西锂矿进行了精细的年代学(Wang et al., 2020; 谭克彬等, 2021, 李永等, 2022; 王威等, 2022; Yan et al., 2022)、地质特征(Wang et al., 2020; 王威等, 2022; 王核等, 2023)和成矿物质以及成矿流体研究(Zhang et al., 2021; Zhou et al., 2021)。研究表明,509道班西锂矿主要赋存于花岗伟晶岩中,与成矿关系密切的白龙山花岗岩形成于215~208 Ma(魏小鹏等, 2018; Wang et al., 2020; 谭克彬等, 2021; Zhou et al., 2021),伟晶岩中铌钽铁矿、独居石和锡石的U-Pb年龄为210~200 Ma(Wang et al., 2020; 谭克彬等, 2021; Zhou et al., 2021; 王核等, 2023)。这些认识为进一步理解花岗伟晶岩型锂元素成矿过程提供了重要的参考。

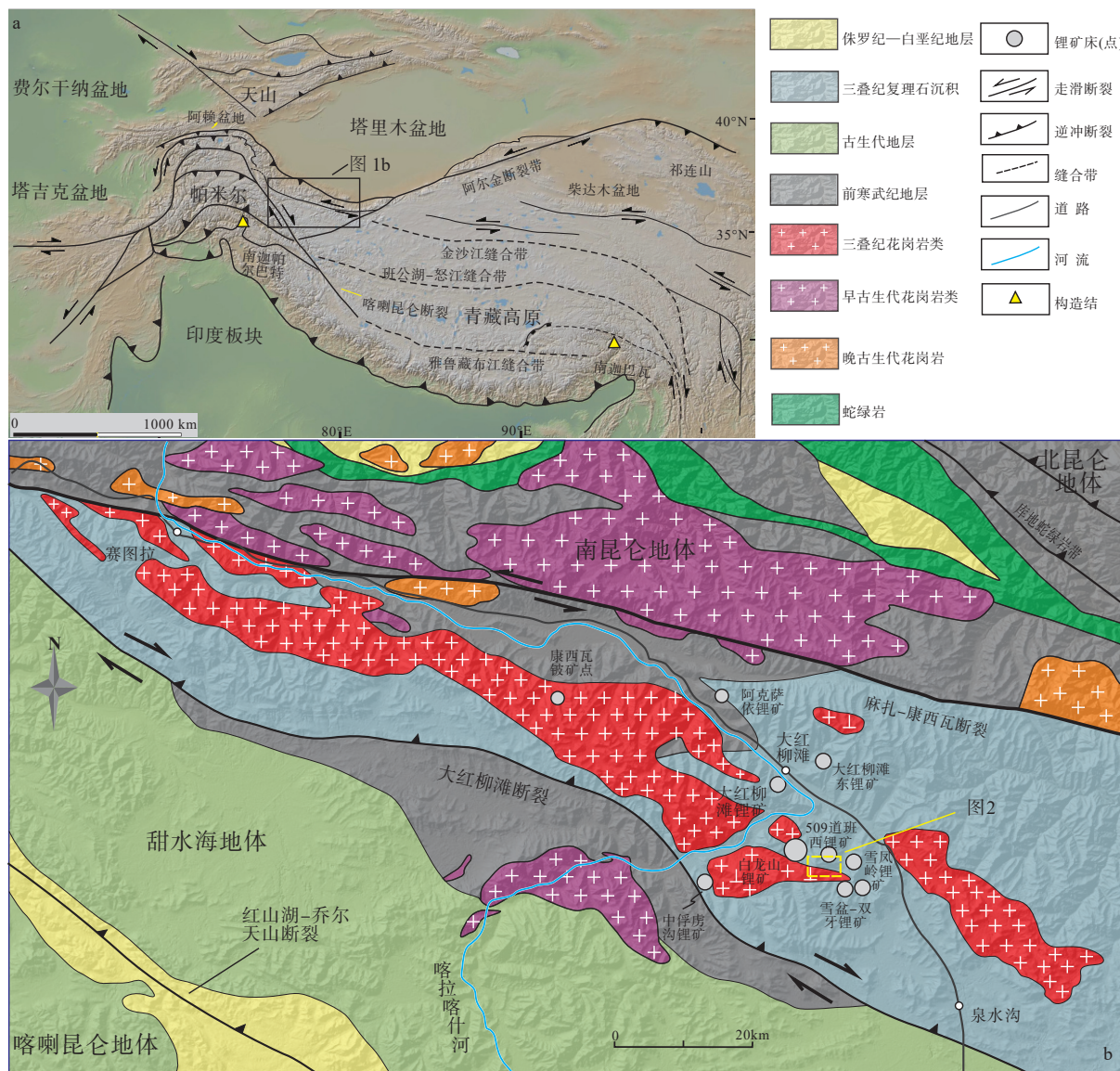
石英是花岗伟晶岩中的主要矿物,其广泛的存在性、较强的抗蚀性和丰富的微量元素等特征,使其成为追踪伟晶岩成矿作用过程的理想对象,并可以指示不同的矿化潜力(Müller et al., 2015, 2021; Rottier and Casanova, 2021; Keyser et al., 2023)。但与锂辉石、锂云母等矿物相比,目前对伟晶岩中石英的研究较少(Müller et al., 2021)。近年来,随着激光质谱仪的广泛使用,对石英原位化学成分的研究日益增多(Wark and Watson, 2006; Thomas et al., 2010; Müller et al., 2021; Keyser et al., 2023)。花岗伟晶岩中石英的变形特征记录了伟晶岩的流变学过程,石英中广泛发育的微量元素(Ge、Rb、B和Be等)与熔

体的分离程度关系密切(Larsen et al., 2000; Müller et al., 2015, 2021),Ti元素浓度对温度较为敏感(Wark and Watson, 2006; Thomas et al., 2010),Al元素含量可能与伟晶岩母岩的性质有关(S型或者A型)(Breiter et al., 2020)。

文章通过系统分析509道班西地区花岗伟晶岩中石英的微量元素和流体包裹体特征,获得了花岗伟晶岩成岩与成矿过程中的温压条件、流体化学组成以及流体来源与演化等信息,结合石英Ti温度计结果,查明了花岗伟晶岩成矿过程中的石英变形行为。

## 1 区域地质背景

大红柳滩地区区域上以库地蛇绿岩带、麻扎-康西瓦断裂带为界,分为北昆仑地体、南昆仑地体和甜水海地块(图1a; Yin and Harrison, 2000; 王核等, 2017, 2021; Wang et al., 2020; Yan et al., 2022)。前寒武纪地层主要包括甜水海岩群、赛图拉岩群和康西瓦岩群,均属于强变形的变质岩组合。晚古生代—中生代沉积地层主要包括黄羊岭群和巴颜喀拉山群(王核等, 2017, 2021)。其中,509道班西矿区主要发育巴颜喀拉山群,总体呈北西向不规则带状展布,为一套浅变质碎屑岩夹少量碳酸盐岩建造;北部与康西瓦岩群呈断层接触关系,南部与甜水海岩群呈断层接触关系(图1b)。区内断裂发育,以北西向断裂最为发育,特别是区域性的麻扎-康西瓦断裂是区内主要的控矿断裂,控制了区内地层和岩浆岩的分布,区内发育的三叠纪赛图拉岩体、大红柳滩岩体和泉水沟岩体等空间展布均受其影响(王核等, 2021; 唐俊林等, 2022; 王威等, 2022)。其中,大红柳滩花岗岩岩体作为509道班西矿区最主要的侵入岩体,呈北西—南东向展布,具有明显的岩相分带,主要包括石英闪长岩、二长花岗岩和二云母花岗岩3类(Yan et al., 2018, 2022; Wang et al., 2020)。锆石U-Pb年代学研究表明,大红柳滩闪长岩的LA-ICP-MS锆石U-Pb年龄为209.9 Ma、二长花岗岩的锆石U-Pb年龄为199~220 Ma、二云母花岗岩的锆石U-Pb年龄为209 Ma,大红柳滩花岗岩形成于晚三叠世古特提斯洋闭合后的后碰撞-后造山



a—西昆仑及邻区大地构造图(据 Yin and Harrison, 2000 修改); b—大红柳滩地区地质图(据王核等, 2017 修改)

图 1 大红柳滩地区大地位置与地质简图

Fig. 1 Geological map of the study area

(a) Tectonic map of West Kunlun and adjacent areas (modified after Yin and Harrison, 2000); (b) Geological map of Dahongliutan area (modified after Wang et al., 2017)

阶段(Yan et al., 2018, 2022; Wang et al., 2020)。

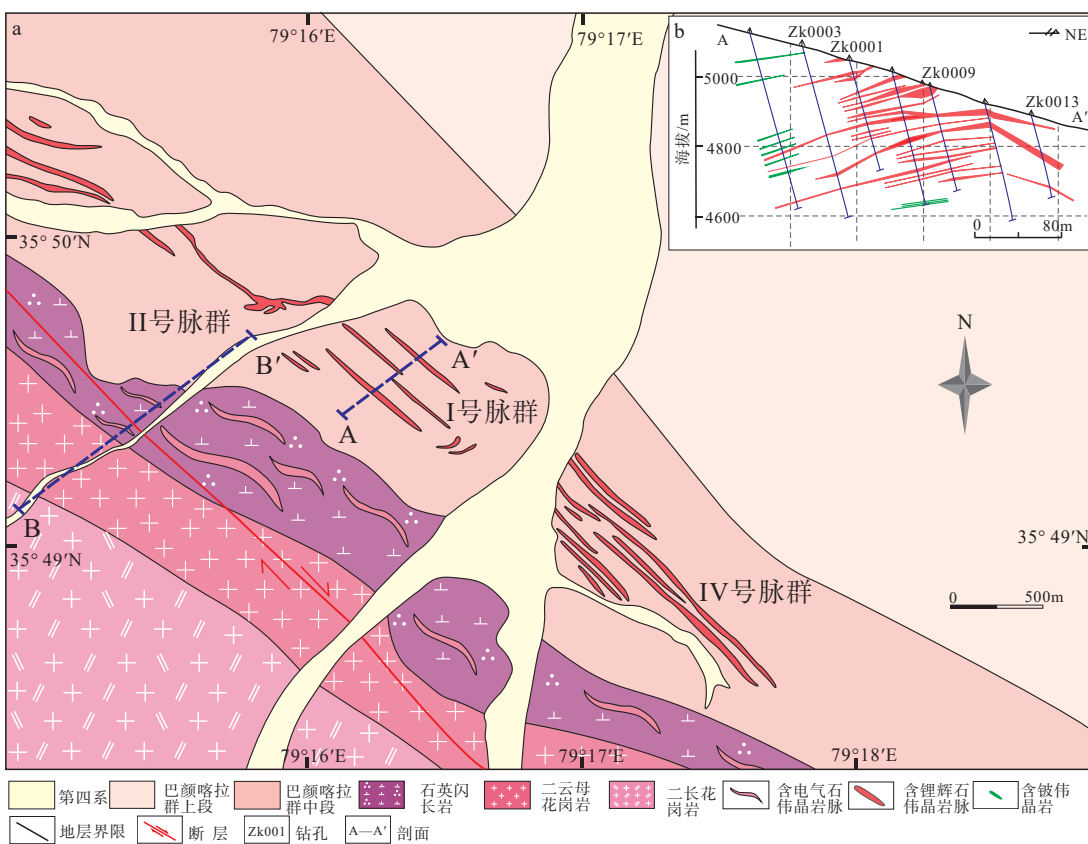
区域上,含稀有金属的伟晶岩脉主要集中于康西瓦-大红柳滩一带,被麻扎-康西瓦断裂和大红柳滩断裂所夹持。稀有矿化的伟晶岩脉主要出露于大红柳滩岩体与三叠系巴颜喀拉山群的外接触带中,主要包括大红柳滩锂矿、白龙山锂矿、509道班西锂矿和雪凤岭锂矿等锂(铍)矿床。其中,509道班西锂(铍)矿床位于大红柳滩岩体的东南部,伟晶岩脉体围绕三叠纪岩体成群成带出现,呈透镜状、串珠状产出,多数顺层侵入,脉长大于25 m的伟晶

岩脉达1000多条,其中含锂辉石、锂云母伟晶岩脉一般长5~1000 m、宽1~30 m,由微斜长石及斜长石、石英、云母和少量电气石、石榴石组成(图1b,图2)。

## 2 矿床地质特征

### 2.1 矿区地质

509道班西锂矿区及其周边岩浆活动频繁,断裂发育,岩石变形强烈,热接触交代变质作用和区域变质作用明显。矿区出露地层为二叠系下—中



a—509道班西地质简图; b—典型勘探线剖面图

图 2 西昆仑 509 道班西地质和典型勘探线剖面图 (据王威等, 2022 修改)

Fig. 2 Geological map and exploration section of the 509 Daobanxi area of West Kunlun (modified after Wang et al., 2022)

(a) Geological map of the 509 Daobanxi area; (b) Exploration section of the 509 Daobanxi area

统黄羊岭群、三叠系巴颜喀拉山群(TB)、新近系泉水沟组( $N_2q$ )及第四系(Q)，其中巴颜喀拉山群为矿区主体地层，也是区内主要的赋矿层位(图 2)。509道班西矿区内地层整体呈一单斜构造，北西—南东向展布，走向为 NW $290^{\circ}\sim315^{\circ}$ ，倾向以北东向为主，倾角为  $50^{\circ}\sim80^{\circ}$ ；局部地层倾向为  $195^{\circ}\sim220^{\circ}$ ，倾角为  $40^{\circ}\sim60^{\circ}$ 。在区域东南部可见层间对称型、宽缓型褶皱构造(图 3)。

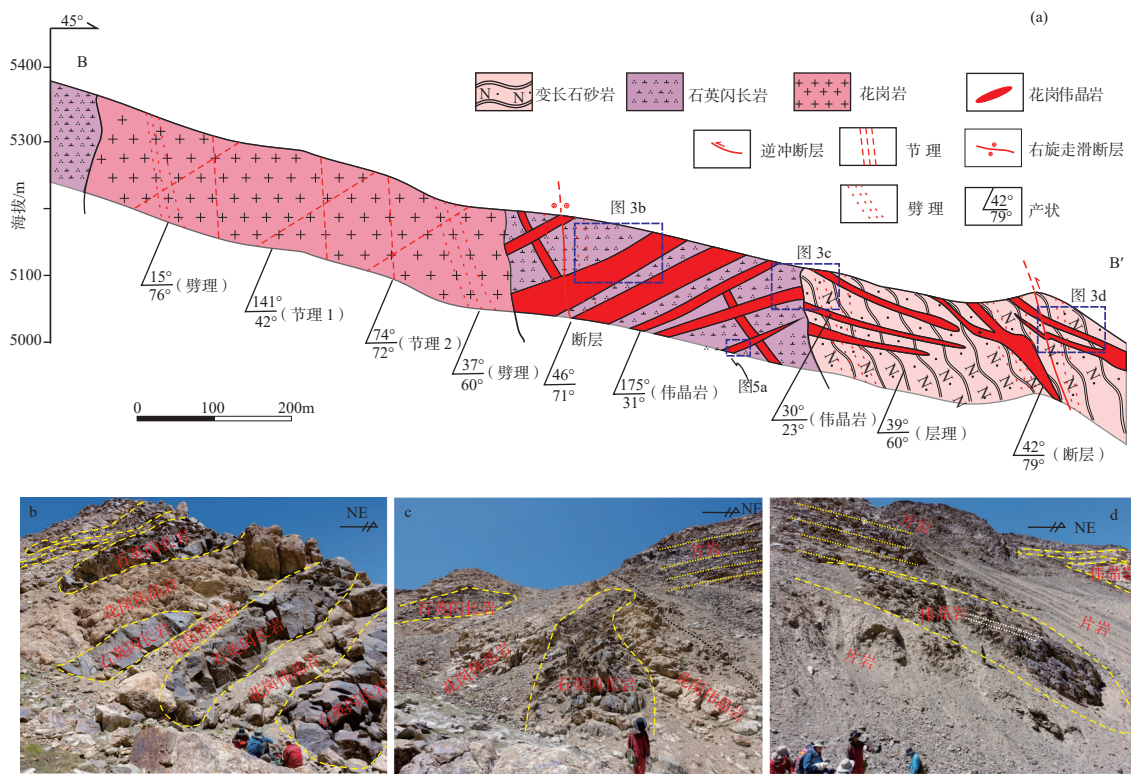
509道班西矿区岩浆活动强烈，酸性侵入岩发育，主要分布在矿区的南部一带，属于大红柳滩岩体的一部分，岩性主要为二云母花岗岩、黑云母花岗闪长斑岩和中—细粒石英闪长岩。矿区内地层整体呈一单斜构造，北西—南东向展布，走向为 NW $290^{\circ}\sim315^{\circ}$ ，倾向以北东向为主，倾角为  $50^{\circ}\sim80^{\circ}$ ；局部地层倾向为  $195^{\circ}\sim220^{\circ}$ ，倾角为  $40^{\circ}\sim60^{\circ}$ 。在区域东南部可见层间对称型、宽缓型褶皱构造(图 3)。

## 2.2 花岗伟晶岩特征

509道班西矿区内地层整体呈一单斜构造，北西—南东向展布，走向为 NW $290^{\circ}\sim315^{\circ}$ ，倾向以北东向为主，倾角为  $50^{\circ}\sim80^{\circ}$ ；局部地层倾向为  $195^{\circ}\sim220^{\circ}$ ，倾角为  $40^{\circ}\sim60^{\circ}$ 。在区域东南部可见层间对称型、宽缓型褶皱构造(图 3)。

变，呈脉状、似层状、透镜状、囊状和分叉树枝状，在走向上可见尖灭再现、分支复合等特征(图 3b—3d)。脉体走向以北西—南东向为主，主体倾向北东，部分呈南西缓倾。

靠近大红柳滩岩体的花岗伟晶岩脉通常不含锂辉石矿物，含矿花岗伟晶岩脉主要集中在岩体与地层接触带的 0~500 m 范围内，总体倾向呈南西向，少量为北东倾向。花岗伟晶岩脉主要呈浅灰色，花岗伟晶结构，碎裂、块状构造；岩石中主要矿物为钠长石(32%)、石英(35%)、斜长石(26%)、电气石(5%~10%)和少量白云母等(图 4)，矿物粒度大小不等，伟晶大小一般为 3~5 cm，个别达 10 cm 以上，伟晶岩脉因遭受挤压明显具有碎裂结构。靠近岩体外接触带 500~1500 m 范围内的花岗伟晶岩脉常含锂辉石矿物，表现出近岩体脉体分布密集、远离岩体则脉体分布稀疏的特征。含锂辉石脉体主要为花岗伟晶结构，块状构造；其主要矿物锂辉石(10%~25%)的单个晶体大小在几厘米至几十厘米不等，一般呈长板状；此外，石英含量为

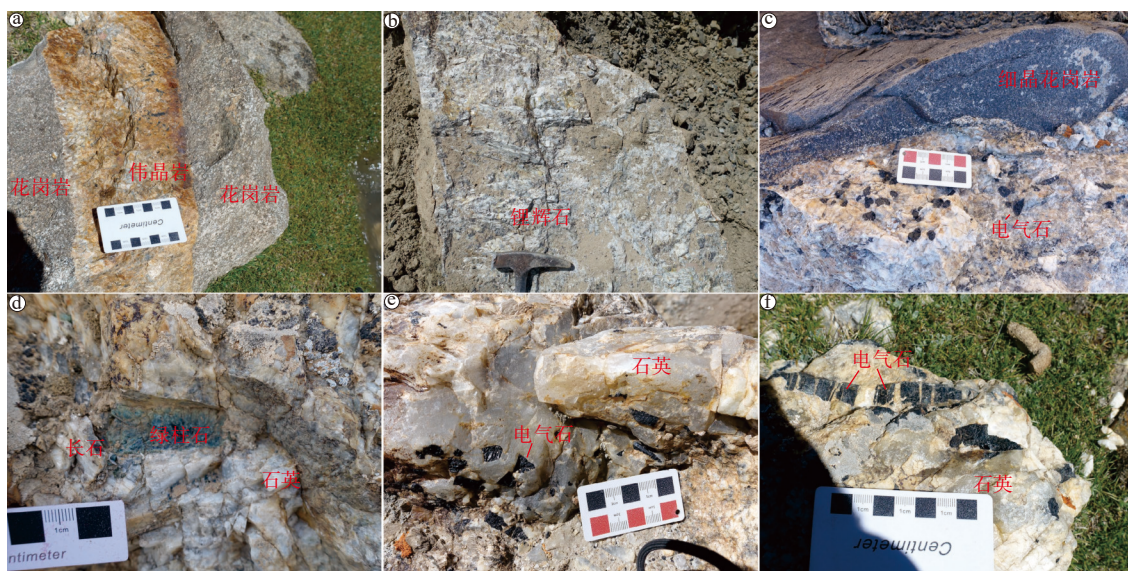


a—剖面特征; b—花岗伟晶岩与石英闪长岩呈互层状产出; c、d—巴颜喀拉山群浅变质岩与花岗伟晶岩接触关系

图3 509道班西锂矿构造剖面与岩脉野外特征(剖面位置见图2)

Fig. 3 Sketch and field photos showing the typical structural profile and field characteristics of the 509 Daobanxi lithium ore deposit (Profile location is shown in Fig.2.)

(a) Sketch of typical structural profile of the 509 Daobanxi area; (b) Photo of quartz diorite and intercalated granite pegmatites; (c and d) Photos showing the intrusive contact relation between meta-sedimentary rocks in Bayankalashan Group and granite pegmatites



a—脉状伟晶岩; b—锂辉石巨晶; c—边部发育细晶花岗岩和电气石; d—过渡带发育长石、石英; e—核部发育石英颗粒; f—电气石布丁化

图4 509道班西锂矿花岗伟晶岩中的典型矿物特征

Fig. 4 Photos showing typical mineral features in granite pegmatites of the 509 Daobanxi lithium deposit

(a) Veined pegmatites; (b) Spodumene megacrysts; (c) Fine-grained granite and oriented tourmaline in the edge zone; (d) Feldspar and quartz in the transition zone; (e) Pure quartz in a core zone; (f) Tourmaline boudinage

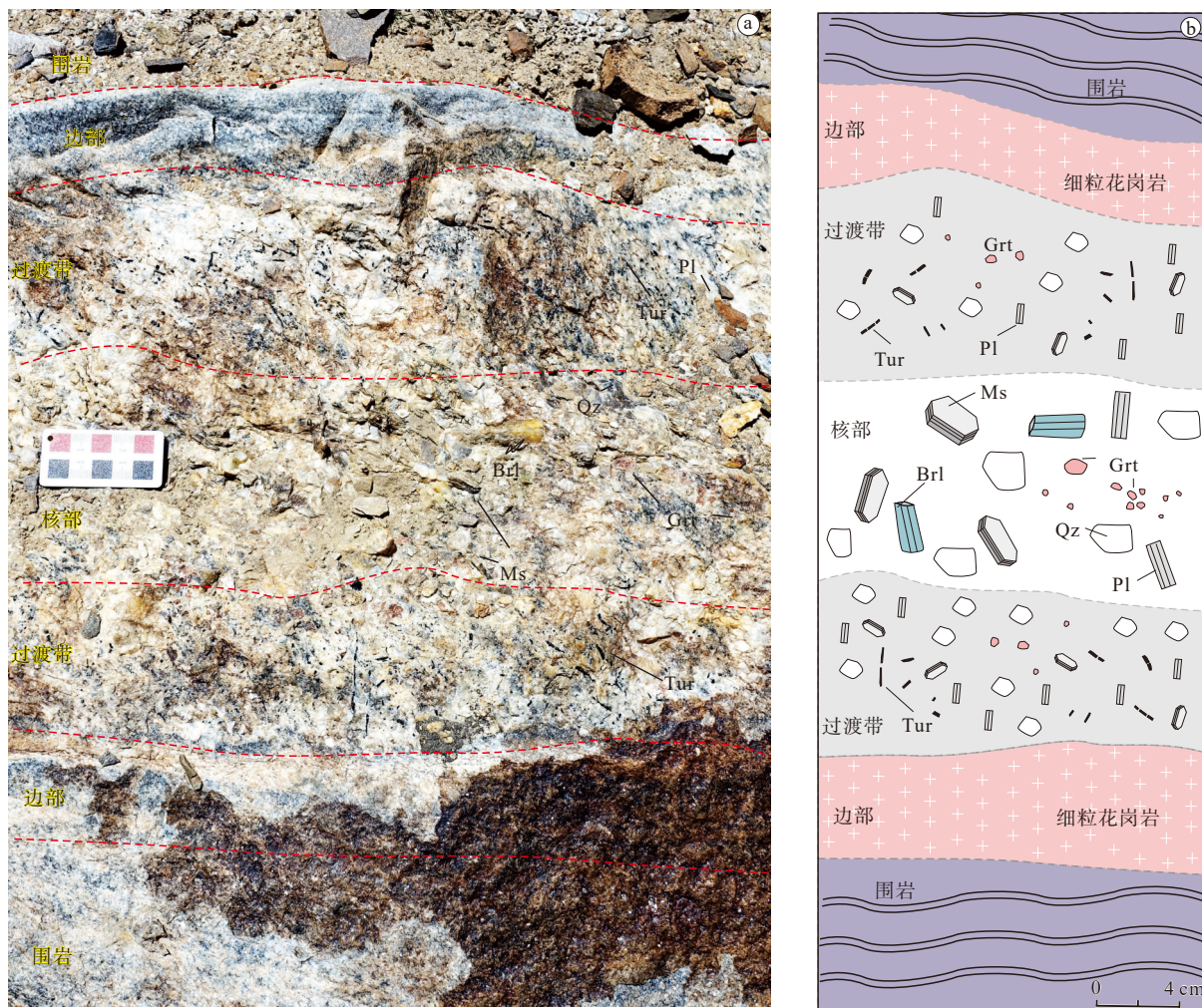
25%~30%、斜长石含量为20%~25%、钾长石约为10%，另含有少量白云母、电气石、磷灰石和石榴子石等；受区域构造应力影响强烈，锂辉石晶体局部变形、碎裂、重结晶。(不)含矿花岗伟晶岩脉在地表一般表现为节理、裂隙发育，或局部弯曲，深部钻孔显示压熔、重结晶。

509道班西花岗伟晶岩内部具有较好的分带性，从围岩到核部依次可以分为：围岩、边部、过渡带和核部(图5; London and Kontak, 2012; London and Morgan, 2012; London, 2018)。其中，围岩与伟晶岩接触的边部常发育细粒花岗岩薄层(厚度为1~3 cm; 图4c, 图5a)，主要矿物为细粒长石-石英-白云母(图5a、5b)；过渡带常以发育梳状结构为特征，钾

长石、电气石和云母等矿物晶体颗粒较边部有所增大；进一步向内常发育有更大的钾长石和石英晶体，局部可见较大的绿柱石和石榴子石等晶体，晶体大小均匀；核部常发育个数更少和颗粒更大的矿物晶体，尤其以石英颗粒较常出现(图4e)。

### 3 花岗伟晶岩中石英的变形特征

509道班西锂矿床中铌钽铁矿、独居石等成矿年代学研究表明，花岗伟晶岩与区域上的二云母花岗岩、石英闪长岩形成时代一致，属于同源花岗岩分异演化的产物(王核等, 2023)。在靠近大红柳滩岩体位置，石英闪长岩与花岗伟晶岩成层状、似层



Pl—斜长石; Tur—电气石; Qz—石英; Brl—绿柱石; Grt—石榴子石; Ms—白云母

a—矿物分带野外特征; b—矿物分带模式图

图5 509道班西锂矿伟晶岩典型矿物分带特征和模式图

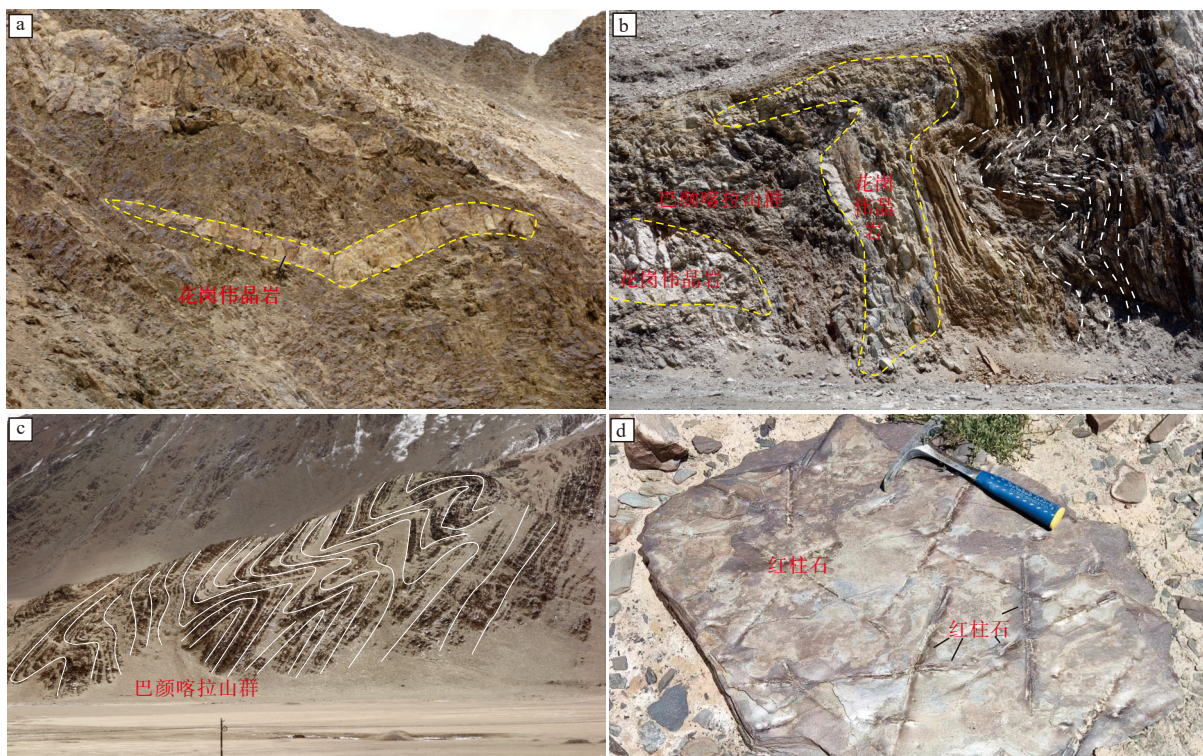
Fig. 5 Typical mineral zoning features and pattern diagram of the pegmatite dike in the 509 Daobanxi lithium deposit, West Kunlun

(a) Field characteristics of mineral zoning; (b) Mineral zoning pattern diagram

Pl—plagioclase; Tur—tourmaline; Qz—quartz; Brl—beryl; Grt—garnet; Ms—muscovite

状、互层状产出, 表明二者存在耦合关系, 属于同构造演化的产物(图3a、3c、3d)。在巴颜喀拉山群中, 花岗伟晶岩主要呈似层状、脉状产出(图6a、6b), 与围岩界限清晰, 围岩主要以褶皱变形为主(图6c), 仅在与花岗岩体接触部位可见红柱石等热接触变质矿物(图6d; 王威等, 2022; 王核等, 2023)。野外

及显微特征均表明, 花岗伟晶岩中的韧性变形仅局限于花岗伟晶岩内部, 代表了伟晶岩在就位过程中受温度、压力改变而发生特定冷却过程的变形特征, 可以限定花岗伟晶岩就位过程的物理性质(Müller et al., 2015, 2021; Rottier and Casanova, 2021; Keyser et al., 2023)。



a—巴颜喀拉山群中发育树状花岗伟晶岩; b—巴颜喀拉山群中发育似层状伟晶岩; c—巴颜喀拉山群褶皱变形; d—接触带发育红柱石等矿物

图6 509道班西巴颜喀拉山群地层及变形特征

Fig. 6 The deformation characteristics of the Bayankalashan Group in the 509 Daobanxi area

(a) Dendritic granitic pegmatite in the Bayankalashan group; (b) Stratified pegmatite in the Bayankalashan group; (c) Folding deformation characteristics of the Bayankalashan Group; (d) Minerals such as andalusite developed along the contact zone of the granites and the Bayankalashan Group

509道班西(不)含矿花岗伟晶岩均发生韧性变形, 其中, 花岗伟晶岩中锂辉石、斜长石主要以脆性变形为主, 破裂发育, 具有刚体变形特征(图7a—7g)。石英主要发育膨凸重结晶(Bulging, BLG)现象(图7a—7g), 石英残斑被细粒的重结晶石英颗粒包围, 并具有亚颗粒旋转现象, 构成石英的核幔构造(图7h、7i); 而白云母普遍变形成云母鱼(图7h、7i)。

## 4 流体包裹体研究

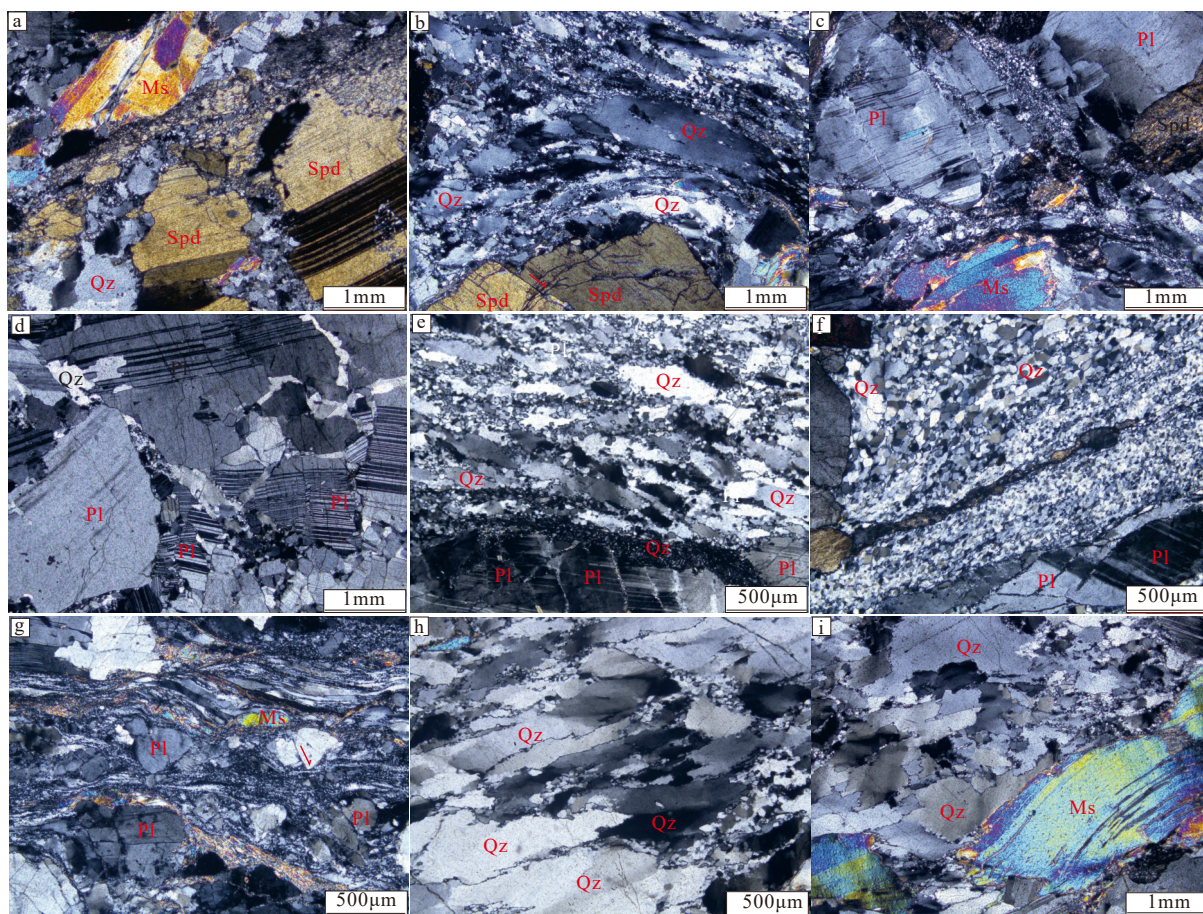
### 4.1 岩相学

509道班西花岗伟晶岩中石英的流体包裹体普

遍较发育, 但流体包裹体较小, 其与主矿物的界限明显, 透明度较好。综合室温下相态分类准则和包裹体冷冻升温过程中的相态变化, 结合激光拉曼光谱分析, 石英中的流体包裹体可分为4种类型。

(1)纯CO<sub>2</sub>气体包裹体(I)。石英中常见纯CO<sub>2</sub>的流体包裹体, 室温状态下呈单一的气相, 多为孤立状产出, 呈椭圆形, 直径一般为1~5 μm, 边界明显。

(2)气液两相包裹体(II)。石英样品中广泛发育气液两相包裹体, 室温状态下该类包裹体由气相和液相组成, 多呈椭圆形、不规则形, 少量为长条形



Spd—锂辉石; Pl—斜长石; Qz—石英; Ms—白云母

a、b—变形伟晶岩中锂辉石发育脆性破裂,石英发育膨凸重结晶;c—g—斜长石等发育破裂,石英发育膨凸重结晶;h、i—石英颗粒发育亚颗粒旋转现象,并发育“核幔构造”,发育云母鱼

图 7 509 道班西锂矿伟晶岩矿物变形特征

Fig. 7 Deformation characteristics of nimerals in pegmatites of the 509 Daobanxi lithium deposit

(a and b) Brittle fracture of spodumene, and expansion and bulging recrystallization of quartz in deformed pegmatite zone; (c–g) Brittle fracture of feldspar, and expansion and bulging recrystallization of quartz in deformed pegmatite zone; (h and i) Muscovite fish, and subgranular rotation developed in quartz grains, exhibiting “nuclear–mantle structure”

Spd—spodumene; Pl—plagioclase; Qz—quartz; Ms—muscovite

与负晶形。包裹体体积变化较小, 直径一般为2~15 μm; 气液比变化较大, 介于5%~50%。包裹体多沿带状分布(图8)。

(3) H<sub>2</sub>O-CO<sub>2</sub>型包裹体(Ⅲ)。该类包裹体在室温状态下呈现气相和液相两相, 根据其在降温-冷冻过程中的变化, 可以进一步分为不显液相的H<sub>2</sub>O-CO<sub>2</sub>型包裹体(Ⅲ<sub>A</sub>型)与含液相的H<sub>2</sub>O-CO<sub>2</sub>型包裹体(Ⅲ<sub>B</sub>型)。这类包裹体数量较少, 直径大小为2~8 μm, 多为椭圆形、不规则形, 呈孤立状产出, 一般为原生包裹体。

(4) 含子矿物的多相包裹体(Ⅳ)。这类包裹体含量极少, 呈椭圆形、不规则、矩形产出; 比其他类

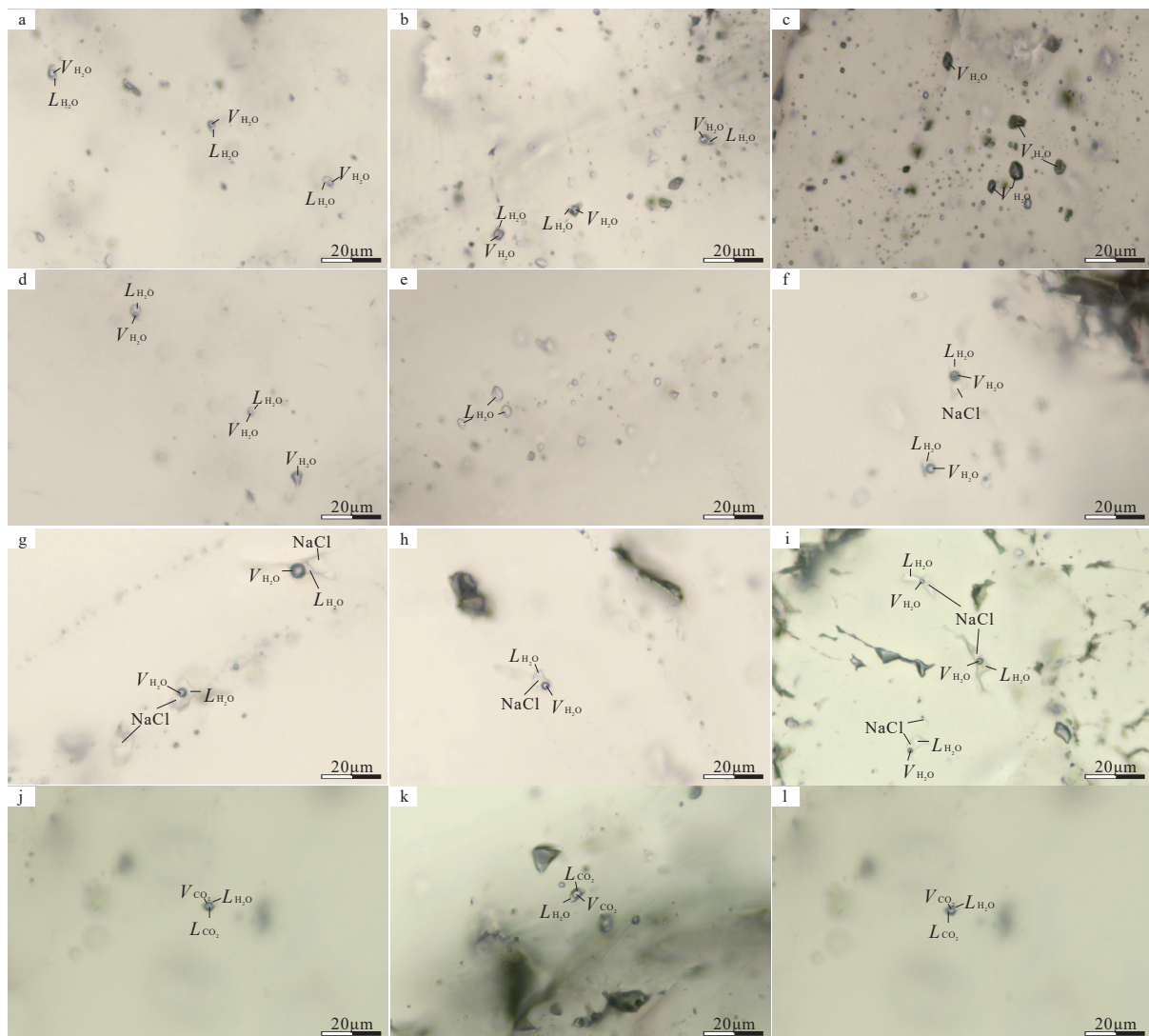
型包裹体大, 直径为5~10 μm。

#### 4.2 拉曼光谱特征

典型流体包裹体的激光拉曼分析表明(图9), 石英样品中整体以水盐系统的两相流体包裹体为主, 包裹体中液相成分主要为H<sub>2</sub>O; 其次为H<sub>2</sub>O-CO<sub>2</sub>型, 气相成分多为CO<sub>2</sub>, 个别包裹体中发现少量的挥发性气体CH<sub>4</sub>。

#### 4.3 显微测温分析

采用均一法、冷冻法对石英中的流体包裹体进一步开展显微测温分析表明, 石英样品的均一温度可分为232~310℃、210~303℃和244~310℃, 对应的平均温度为273℃、260℃和283℃(表1)。



$V_{CO_2}$ —气相  $CO_2$ ;  $L_{CO_2}$ —液相  $CO_2$ ;  $L_{H_2O}$ —液相  $H_2O$ ;  $V_{H_2O}$ —气相  $H_2O$ ; NaCl—NaCl子矿物

a、b—气液两相包裹体; c—富气相包裹体群; d—气液包裹体与富气相包裹体共存; e—富液相包裹体群; f—气液两相包裹体和含子矿物的三相包裹体; g、h—含子矿物的三相包裹体; i—发育在裂隙中的含子矿物的三相包裹体; j—l—含  $CO_2$  包裹体

图 8 509 道班西花岗伟晶岩中石英流体包裹体显微照片

Fig. 8 Microphotos showing characteristics of quartz inclusion in pegmatites of the 509 Daobanxi lithium deposit

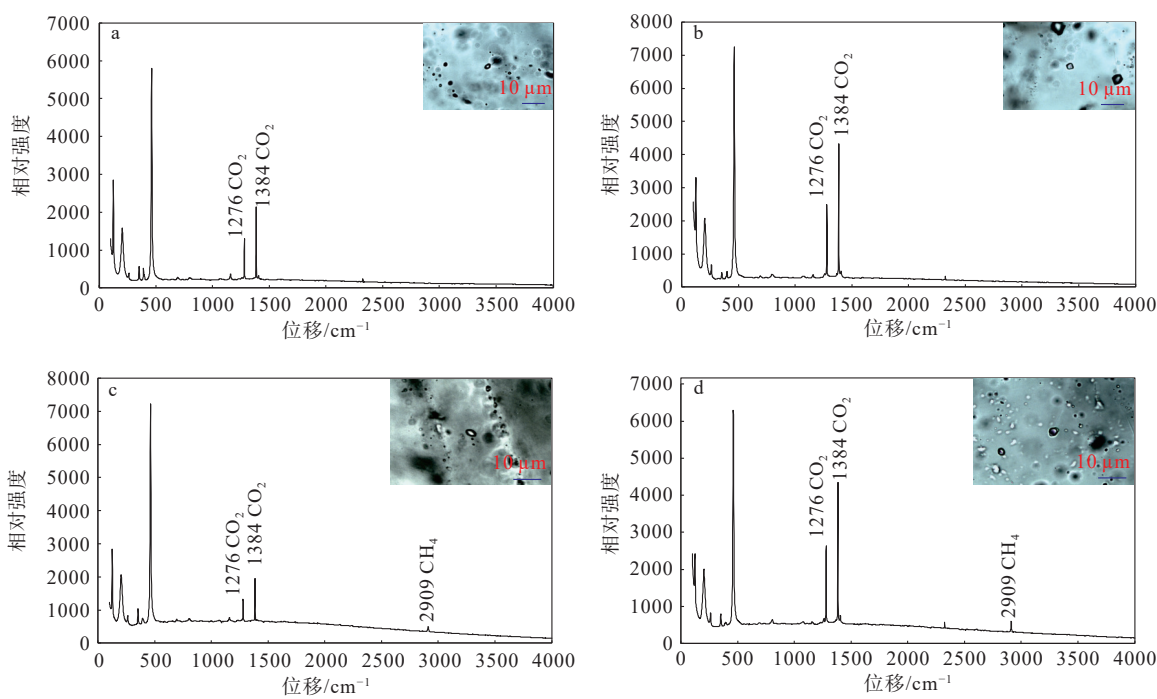
(a and b) Gas-liquid two-phase inclusions; (c) Gas-rich phase inclusion group; (d) Coexistence of gas-liquid inclusions and gas-rich inclusions; (e) Liquid-rich phase inclusion group; (f) Gas-liquid two-phase inclusions and three-phase inclusions containing daughter minerals; (g and h) Three-phase inclusions containing daughter minerals; (i) Three-phase inclusions containing daughter minerals developed in fractures; (j-l)  $CO_2$ -bearing inclusions

$V_{CO_2}$ —gas phase  $CO_2$ ;  $L_{CO_2}$ —liquid phase  $CO_2$ ;  $L_{H_2O}$ —liquid phase  $H_2O$ ;  $V_{H_2O}$ —gas phase  $H_2O$ ; NaCl—NaCl daughter minerals

## 5 花岗伟晶岩石英 Ti 温度计测试

为揭示石英条带 Ti 含量的成分分带, 首先对变形成花岗伟晶岩样品中的石英进行了阴极发光成像(CL)分析, 该实验在锆年领航科技有限公司完成。石英中 Ti 含量的测定在岩石圈演化国家重点实验

室(中国科学院地质与地球物理研究所)完成, 实验仪器采用安捷伦电感耦合等离子体-质谱仪(Agilent 7900 ICP-MS)和 GoherentGeolas 193 nm 准分子激光。石英样品表面经过抛光, 厚度约为 100  $\mu m$ 。激光频率为 10 Hz, 能量密度为 10  $J/cm^2$ , 光斑尺寸为 44  $\mu m$ 。质量校准采用 NIST SRM610、GSE、BCR-2G 外标, 每 12 个分析点分析 2 次。石英 Ti 含量结果见



a、b—CO<sub>2</sub>气相包裹体; c、d—CO<sub>2</sub>气相包裹体,且含少量CH<sub>4</sub>

图9 509道班西锂矿伟晶岩中石英包裹体拉曼图谱特征

Fig. 9 Raman spectra characteristics of quartz fluid inclusions in pegmatites of the 509 Daobanxi lithium deposit  
(a and b) CO<sub>2</sub> gas inclusions; (c and d) CO<sub>2</sub> gas inclusions with small amounts of CH<sub>4</sub>

表1 509道班西锂矿伟晶岩中石英包裹体测温数据

Table 1 Temperature data of quartz fluid inclusions in pegmatites of the 509 Daobanxi lithium deposit

赋存矿物	样品数量	包裹体类型	均一温度/℃	冰点/℃	CO <sub>2</sub> 络合物融化温度/℃	盐度
石英	36	II	232~310(273)	-3.3~-11(-6.6)	—	6.3~14.95(9.5)
石英	30	III	210~303(260)	-3.6~-9.1(-6.36)	5.9~8.9(7.3)	2.23~4.64(5.25)
石英	4	IV	244~310(283)	-5.5~-9.7(-7.4)	—	7.6~12.5(9.7)

注:()内为平均值

表2. Ti含量的不确定度小于10%。

石英的CL图像通常可以反映其Ti浓度的变化(Kohn and Northrup, 2009)。509道班西花岗伟晶岩样品中石英条带的CL图像没有明显的分带性,表明Ti含量在石英变形中达到相对平衡状态(图10)。在Zk2707-9和Zk1107-2样品的石英条带上共分析了64个测试点(表2),并使用Thomas et al.(2010)版本的TitaniQ温度计计算了每个点的变形温度。计算时考虑到显微镜观察不能确定石英是否属于Ti饱和体系,因此将石英样品的TiO<sub>2</sub>活性(aTiO<sub>2</sub>)分别设定为1.0、0.8和0.6。同时依据Zhang et al.(2022)估算的压力值,将韧性变形的压力条件设定为3.7 kbar。2个样品的石英Ti含量相对均匀(图10),分别为 $1.03 \times 10^{-6} \sim 7.67 \times 10^{-6}$ 和 $1.04 \times 10^{-6} \sim 6.75 \times 10^{-6}$ (表2);

相应地,由TitaniQ温度计计算出的变形温度也相对一致(图10),ZK2707-9样品的平均温度分别为371 °C(aTiO<sub>2</sub>=1)、382 °C(aTiO<sub>2</sub>=0.8)、398 °C(aTiO<sub>2</sub>=0.6);ZK1107-2样品平均温度为351 °C(aTiO<sub>2</sub>=1)、362 °C(aTiO<sub>2</sub>=0.8)、377 °C(aTiO<sub>2</sub>=0.6)。考虑到与伟晶岩典型矿物发生变形的对应温度范围(图11),结合石英Ti温度计计算结果,此次将石英韧性变形的温度集中在377~398 °C(aTiO<sub>2</sub>=0.6),同时以398 °C作为石英韧性变形的温度标准进行探讨。

## 6 讨论

### 6.1 花岗伟晶岩变形温度的约束

温度是影响岩石流变学性质、进而影响变形组

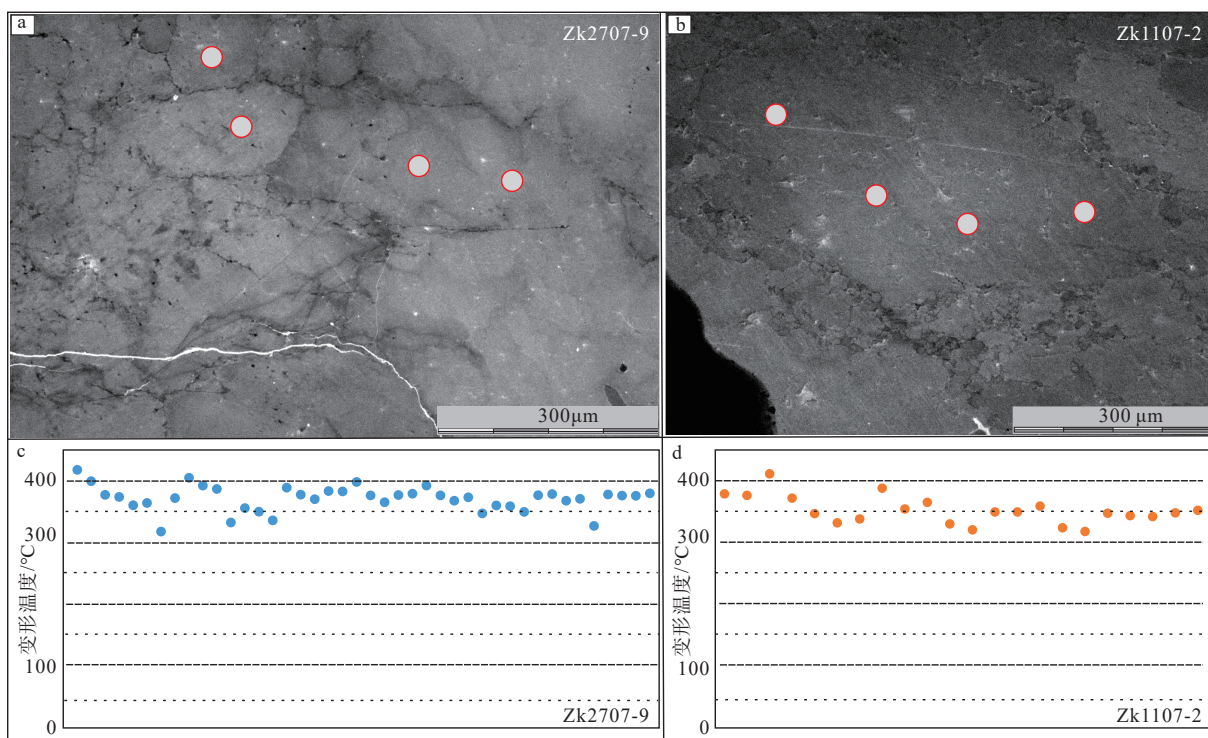
表2 509道班西锂矿伟晶岩中石英的变形温度

Table 2 Deformation temperature of quartz in pegmatites of the 509 Daobanxi lithium deposit

样品号	测点	Ti/ $\times 10^{-6}$	P/kbar	T/°C (aTiO <sub>2</sub> =1)	T/°C (aTiO <sub>2</sub> =0.8)	T/°C (aTiO <sub>2</sub> =0.6)	测点	Ti/ $\times 10^{-6}$	P/kbar	T/°C (aTiO <sub>2</sub> =1)	T/°C (aTiO <sub>2</sub> =0.8)	T/°C (aTiO <sub>2</sub> =0.6)
	A1	7.67	3.7	418	431	449	A24	3.60	3.7	376	388	404
	A2	5.54	3.7	399	412	429	A25	2.90	3.7	365	376	392
	A3	3.67	3.7	377	389	405	A26	3.64	3.7	377	388	404
	A4	3.44	3.7	374	385	401	A27	3.80	3.7	379	391	407
	A5	2.63	3.7	360	371	386	A28	4.87	3.7	392	404	421
	A6	2.82	3.7	364	375	390	A29	3.61	3.7	376	388	404
	A7	1.03	3.7	317	327	340	A30	3.05	3.7	368	379	394
	A8	3.31	3.7	372	383	399	A31	3.39	3.7	373	385	400
	A9	6.11	3.7	405	418	435	A33	1.99	3.7	347	357	372
	A11	4.88	3.7	392	405	421	A34	2.62	3.7	360	371	386
Zk2707-9	A12	4.40	3.7	387	399	415	A35	2.55	3.7	359	370	385
	A13	1.45	3.7	332	342	356	A36	2.10	3.7	349	360	375
	A14	2.38	3.7	355	366	381	A37	3.61	3.7	376	388	404
	A16	2.11	3.7	349	360	375	A38	3.75	3.7	378	390	406
	A17	1.56	3.7	335	346	360	A39	3.04	3.7	367	379	394
	A18	4.56	3.7	389	401	417	A40	3.24	3.7	371	382	398
	A19	3.70	3.7	377	389	405	A41	1.28	3.7	326	336	350
	A20	3.20	3.7	370	382	397	A42	3.71	3.7	378	389	405
	A21	4.13	3.7	383	395	412	A43	3.59	3.7	376	388	403
	A22	4.08	3.7	383	395	411	A44	3.57	3.7	376	387	403
	A23	5.41	3.7	398	410	427	A45	3.85	3.7	380	391	408
	A46	3.74	3.7	378	390	406	A57	1.11	3.7	320	330	343
	A47	3.57	3.7	376	387	403	A58	2.08	3.7	349	360	374
	A48	6.75	3.7	410	423	441	A59	2.08	3.7	349	360	374
	A49	3.28	3.7	371	383	399	A60	2.54	3.7	358	370	385
	A50	1.97	3.7	346	357	371	A70	1.20	3.7	323	333	347
Zk1107-2	A51	1.43	3.7	331	341	355	A71	1.04	3.7	317	327	340
	A52	1.64	3.7	337	348	362	A72	2.00	3.7	347	358	372
	A53	4.45	3.7	387	399	416	A75	1.84	3.7	343	354	368
	A54	2.31	3.7	354	365	379	A76	1.78	3.7	341	352	366
	A55	2.86	3.7	364	376	391	A77	2.02	3.7	347	358	373
	A56	1.37	3.7	329	340	353	A78	2.21	3.7	351	362	377

构的关键因素之一(Passchier and Trouw, 2005; Platt and Behr, 2011; London, 2018)。锂辉石、斜长石和石英变形特征的微观证据表明, 糜棱岩化伟晶岩发生变形的温度为300~400 °C(图11a; Passchier and Trouw, 2005; Fossen and Cavalcante, 2017)。此次石英Ti温度计计算出的变形温度为371~398 °C和351~377 °C, 与微观组构所指示的变形温度范围一

致。伟晶岩中石英包裹体的均一温度平均为260~283 °C, 可能记录了石英变形晚阶段的温度。已有研究表明, 花岗伟晶岩就位过程中短时间内温度就可以从398 °C降低到260 °C( $\Delta T \approx 150$  °C; London and Morgan, 2012)。文中石英变形温度所显示出的快速冷却过程( $\Delta T \approx 150$  °C)表明, 509道班西花岗伟晶岩在就位过程中具有超冷却的特征(图11b)。在高应

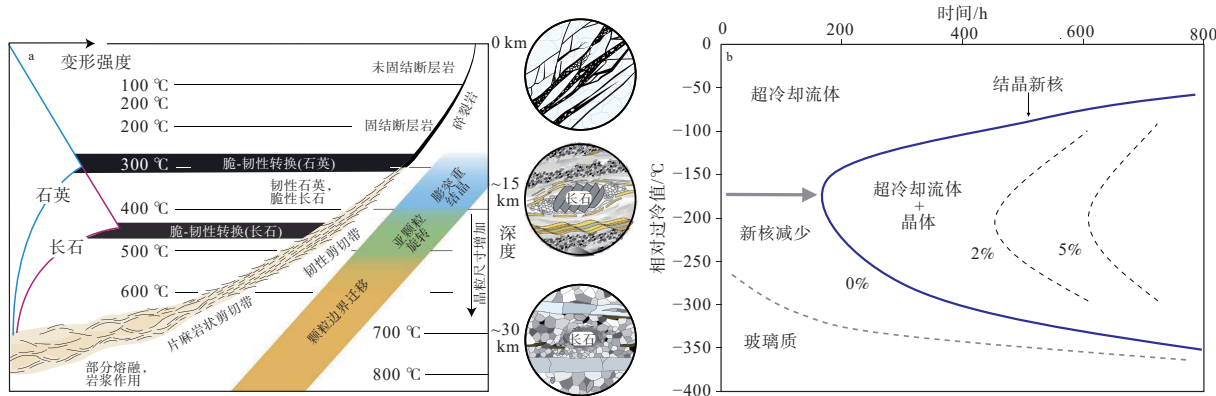


a—b—石英 CL 图像及典型测试点; c—d—石英 Ti 温度计计算结果

图 10 509 道班西锂矿花岗伟晶岩中石英变形温度图解

Fig. 10 Illustration of quartz deformation temperature in pegmatites of the 509 Daobanxi lithium deposit

(a and b) Cathodoluminescence images of quartz and typical test points; (c and d) Results of titanium thermometry on quartz



a—不同构造层次典型矿物的变形特征(Fosson and Cavalcante, 2017); b—流体超冷却与晶体成核程度图(London and Morgan, 2012)

图 11 不同构造层次典型矿物的变形特征和流体超冷却与晶体成核程度图

Fig. 11 Diagrams illustrating the typical mineral deformation characteristics at different tectonic levels and the crystal-nucleation delay and the onset of undercooling time

(a) Typical mineral deformation characteristics at different tectonic levels (Fosson and Cavalcante, 2017); (b) The crystal-nucleation delay and the onset of undercooling time (London and Morgan, 2012)

力和较低温度条件下, 动态重结晶(GBM)导致的晶粒粒径减小深刻地改变了岩石流变学性质, 也参与了随后的构造演化(Platt and Behr, 2011)。重结晶颗粒的大小则主要受成核过程的影响, 可能受旧晶粒中亚晶粒或位错细胞大小的控制(Platt and Behr, 2011)。

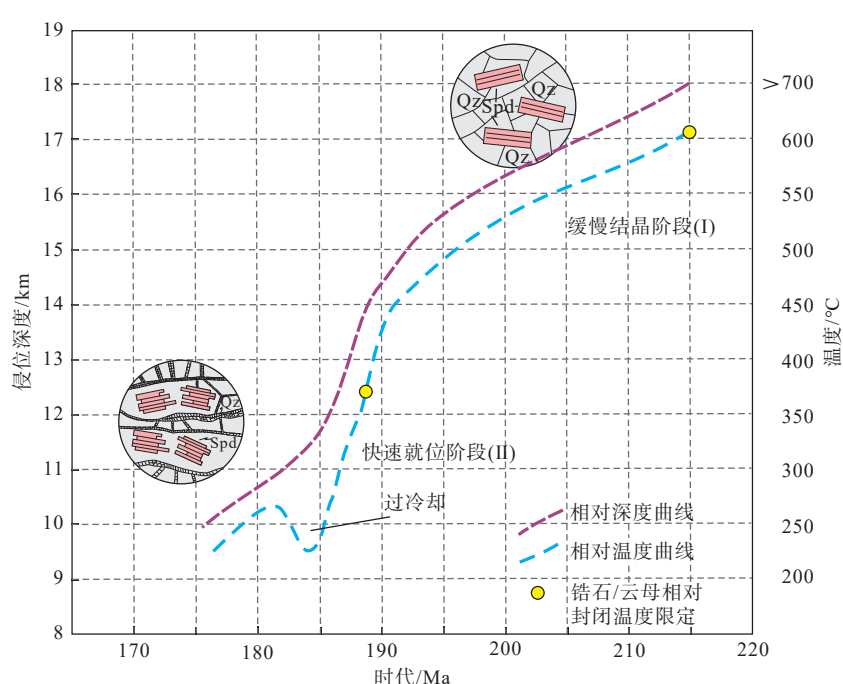
## 6.2 花岗伟晶岩变形与成矿作用

研究表明花岗伟晶岩的就位深度一般在 6~9 km(Brisbin, 1986; Rubin, 1995), 509 道班西锂矿伟晶岩岩脉的数量在距离三叠纪岩体约 1 km 外迅速减少, 侵入于沉积(变质)地层中的伟晶岩脉通常呈透

镜状或“X”形, 具有较为复杂的空间形态(图2)。

509道班西地区的全岩地球化学和锂同位素研究表明, 富锂矿伟晶岩是花岗质岩浆演化晚期阶段流体分离结晶的产物(Fan et al., 2020; 周起凤等, 2023; 许志琴等, 2023)。花岗伟晶岩与围岩接触的边部发育的细粒花岗岩主要由岩浆热液经历二次气液相分离形成的残余熔体过冷却结晶形成(洪涛等, 2023)。伴随花岗岩岩浆的高度分离结晶作用, 富锂伟晶岩在相对封闭的岩浆-热液体系中经历了广泛的矿物-流体相互作用, 导致锂辉石等物质的析出和再沉淀过程, 而熔体不混熔可能是锂矿超常富集的启动机制(Fan et al., 2020; 许志琴等, 2023)。伟晶岩石英条带中的港湾状、锯齿状边界暗示(图4e、4f), 伟晶岩的就位是快速冷却过程的产物, 而超临界流体快速扩散过程导致锂元素进一步富集(Fan et

al., 2020)。509道班西地区的石榴石地球化学表明, 从白云母花岗岩—(无)贫矿伟晶岩—含矿伟晶岩, 成矿流体的分异程度逐渐增加, 含矿伟晶岩的分异演化程度最高(Zhang et al., 2022)。锂同位素扩散模拟过程表明, 高冷却速率有利于富锂伟晶岩的形成(Zhou et al., 2021); 而温度从 $\sim 400\text{ }^{\circ}\text{C}$ 降到 $\sim 260\text{ }^{\circ}\text{C}$ 的超冷却过程( $\Delta T = \pm 140\text{ }^{\circ}\text{C}$ ), 会造成伟晶岩中结晶矿物新核的数量较少, 更有利于形成粗大的石英等矿物颗粒(图11b, 图12), 形成的伟晶岩脉具有显著的特征和独特的岩石结构和矿物组合的空间分带, 超冷却在伟晶岩就位过程中具有重要的作用(London and Morgan, 2012; Zhou et al., 2021); 因此, 超冷却作用对伟晶岩中锂元素的富集和就位同样具有重要意义。



Spd—锂辉石; Qz—石英; 深度与温度曲线是结合此次研究和王威等(2022)的年代学研究限定的

图12 西昆仑地区509道班西花岗伟晶岩就位示意图

Fig. 12 Diagram showing the emplacement of granite pegmatites in the 509 Daobanxi deposit, West Kunlun  
Spd-spodumene; Qz-quartz; The depth and temperature curves are constrained by the results of this study and the chronology research by Wang et al. (2022).

## 7 结论

(1) 509道班西锂矿的花岗伟晶岩中锂辉石主要以脆性破裂为主, 石英主要发育膨凸重结晶现象, 部分发育核幔构造, 糜棱岩化伟晶岩的变形温

度为 $300\sim 400\text{ }^{\circ}\text{C}$ 。伟晶岩中石英Ti温度计计算的变形温度为 $371\sim 398\text{ }^{\circ}\text{C}$ 和 $351\sim 377\text{ }^{\circ}\text{C}$ , 与微观结构所指示的变形温度范围一致。

(2) 花岗伟晶岩石英中的流体包裹体以气液两相为主, 液相成分主要为 $\text{H}_2\text{O}$ ; 其次为 $\text{H}_2\text{O}-\text{CO}_2$ 型,

气相主要为 CO<sub>2</sub>, 少量为挥发性气体 H<sub>2</sub>S 与 CH<sub>4</sub>。石英包裹体的均一温度平均为 260~283 °C, 可能记录了石英变形晚阶段的温度。而伟晶岩从 398 °C 到 260 °C 的温度差则表明其具有超冷却的特征。

(3) 509 道班西锂矿伟晶岩的就位是快速冷却过程的产物, 超冷却花岗伟晶岩就位过程具有重要的作用, 可形成伟晶岩脉所有显著特征和独特的岩石结构和矿物组合的空间分带。

## References

- BREITER K, ĎURIŠOVÁ J, DOSBABA M, 2020. Chemical signature of quartz from S- and A-type rare-metal granites-A summary[J]. *Ore Geology Reviews*, 125: 103674.
- BRISBIN W C, 1986. Mechanics of pegmatite intrusion[J]. *American Mineralogist*, 71(3-4): 644-651.
- CHEN M, WANG H, ZHANG X Y, et al., 2022. Judgment of metallogenic potential of Kangxiwa pegmatite in Xinjiang: evidence from zircon U-Pb geochronology, geochemistry and Lu-Hf isotope[J]. *Acta Petrologica Sinica*, 38(7): 2095-2112. (in Chinese with English abstract)
- FAN J J, TANG G J, WEI G J, et al., 2020. Lithium isotope fractionation during fluid exsolution: implications for Li mineralization of the Bailongshan pegmatites in the west Kunlun, NW Tibet[J]. *Lithos*, 352-353: 105236.
- FOSSEN H, CAVALCANTE G C G, 2017. Shear zones-a review[J]. *Earth Science Reviews*, 171: 434-455.
- HONG T, ZHAI M G, WANG Y J, et al., 2023. Coupling relationship between the stability of Li/Be complexes and Li/Be differential enrichment in granitic pegmatites—an experimental study[J]. *Earth Science Frontiers*, 30(5): 93-105. (in Chinese with English abstract)
- KEYSER W, MÜLLER A, KNOLL T, et al., 2023. Quartz chemistry of lithium pegmatites and its petrogenetic and economic implications: examples from Wolfsberg (Austria) and Moylisha (Ireland)[J]. *Chemical Geology*, 630: 121507.
- KOHN M J, NORTHRUP C J, 2009. Taking mylonites' temperatures[J]. *Geology*, 37(1): 47-50.
- LARSEN R B, POLVÉ M, JUVE G, 2000. Granite pegmatite quartz from Evje-Iveland: trace element chemistry and implications for the formation of high-purity quartz[J]. *Norges Geologiske Undersø gelse Bulletin*, 436: 57-65.
- LI J K, LI P, CHEN Z Y, 2023. Metallogenic regularity, prediction and assessment of strategic metal mineral resources such as lithium and beryllium: preface[J]. *Acta Petrologica Sinica*, 39(7): 1881-1886. (in Chinese with English abstract)
- LI Y, WANG W, DU X F, et al., 2022. <sup>40</sup>Ar/<sup>39</sup>Ar dating of muscovite of the west 509 Daoban Li-Be rare metal deposit in the west Kunlun orogenic belt and its limitation to regional mineralization[J]. *Geology in China*, 49(6): 2031-2033. (in Chinese with English abstract)
- LONDON D, KONTAK D J, 2012. Granitic pegmatites: scientific wonders and economic bonanzas[J]. *Elements*, 8(4): 257-261.
- LONDON D, MORGAN VI G B, 2012. The pegmatite puzzle[J]. *Elements*, 8(4): 263-268.
- LONDON D, 2018. Ore-forming processes within granitic pegmatites[J]. *Ore Geology Reviews*, 101: 349-383.
- MÜLLER A, IHLEN P M, SNOOK B, et al., 2015. The chemistry of quartz in granitic pegmatites of southern Norway: petrogenetic and economic implications[J]. *Economic Geology*, 110(7): 1737-1757.
- MÜLLER A, KEYSER W, SIMMONS W B, et al., 2021. Quartz chemistry of granitic pegmatites: implications for classification, genesis and exploration[J]. *Chemical Geology*, 584: 120507.
- PASSCHIER C W, TROUW R A J, 2005. *Microtectonics*[M]. 2nd ed. Berlin: Springer: 31-60.
- PLATT J P, BEHR W M, 2011. Grainsize evolution in ductile shear zones: implications for strain localization and the strength of the lithosphere[J]. *Journal of Structural Geology*, 33(4): 537-550.
- ROTTIER B, CASANOVA V, 2021. Trace element composition of quartz from porphyry systems: a tracer of the mineralizing fluid evolution[J]. *Mineralium Deposita*, 56(5): 843-862.
- RUBIN A M, 1995. Getting granite dikes out of the source region[J]. *Journal of Geophysical Research: Solid Earth*, 100(B4): 5911-5929.
- TAN K B, GUO Q M, GUO Y M, 2021. U-Pb age of granite from Li-beryllium polymetallic deposit and its tectonic significance in 509 Daobanxi of Hotan, Xinjiang[J]. *Nonferrous Metals of Xinjiang*, 44(2): 6-10. (in Chinese)
- TANG J L, KE Q, XU X W, et al., 2022. Magma evolution and mineralization of Longmenshan lithium-beryllium pegmatite in Dahongliutan area, west Kunlun[J]. *Acta Petrologica Sinica*, 38(3): 655-675. (in Chinese with English abstract)
- TANG W C, DUAN W, ZOU L, et al., 2022. A method for locating ore bodies by geochemical indexes of pegmatite-type lithium deposits in the Ke'eryin area, western Sichuan, China[J]. *Journal of Geomechanics*, 28(5): 765-792. (in Chinese with English abstract)
- THOMAS J B, WATSON E B, SPEAR F S, et al., 2010. TitaniQ under pressure: the effect of pressure and temperature on the solubility of Ti in quartz[J]. *Contributions to Mineralogy and Petrology*, 160(5): 743-759.
- WANG D H, DAI H Z, LIU S B, et al., 2022. New progress and trend in ten aspects of lithium exploration practice and theoretical research in China in the past decade[J]. *Journal of Geomechanics*, 28(5): 743-764. (in Chinese with English abstract)
- WANG H, LI P, MA H D, et al., 2017. Discovery of the Bailongshan super-large lithium-rubidium deposit in Karakorum, Hetian, Xinjiang, and its prospecting implication[J]. *Geotectonica et Metallogenica*, 41(6): 1053-1062. (in Chinese with English abstract)
- WANG H, GAO H, ZHANG X Y, et al., 2020. Geology and geochronology of the super-large Bailongshan Li-Rb-(Be) rare-metal pegmatite deposit, west Kunlun orogenic belt, NW China[J]. *Lithos*, 360-361: 105449.
- WANG H, XU Y G, YAN Q H, et al., 2021. Research progress on Bailongshan pegmatite type lithium deposit, Xinjiang[J]. *Acta Geologica Sinica*, 95(10): 3085-3098. (in Chinese with English abstract)
- WANG H, HUANG L, MA H D, et al., 2023. Geological characteristics and metallogenic regularity of lithium deposits in Dahongliutan-Bailongshan area, west Kunlun, China[J]. *Acta Petrologica Sinica*, 39(7): 1931-1949.

- (in Chinese with English abstract)
- WANG W, DU X F, LIU W, et al., 2022. Geological characteristic and discussion on metallogenetic age of the west 509-Daoban Li-Be rare metal deposit in the west Kunlun orogenic belt[J]. *Acta Petrologica Sinica*, 38(7): 1967-1980. (in Chinese with English abstract)
- WARK D A, WATSON E B, 2006. TitaniQ: a titanium-in-quartz geothermometer[J]. *Contributions to Mineralogy and Petrology*, 152(6): 743-754.
- WEI X P, WANG H, ZHANG X Y, et al., 2018. Petrogenesis of Triassic high-Mg diorites in western Kunlun orogen and its tectonic implication[J]. *Geochimica*, 47(4): 363-379. (in Chinese with English abstract)
- XU Y G, WANG R C, WANG C Y, et al., 2021. Highly fractionated granites and rare-metal mineralization[J]. *Lithos*, 398-399: 106262.
- XU Z Q, ZHU W B, ZHENG B H, et al., 2023. New ore-controlling theory of "multilayered domal granitic sheets" of the Jiajika pegmatite-type lithium deposit: the major discoveries of the "Jiajika pegmatite-type lithium deposit scientific drilling project (JSD)" [J]. *Acta Geologica Sinica*, 97(10): 3133-3146. (in Chinese with English abstract)
- YAN Q H, QIU Z W, WANG H, et al., 2018. Age of the Dahongliutan rare metal pegmatite deposit, west Kunlun, Xinjiang (NW China): constraints from LA-ICP-MS U-Pb dating of columbite-(Fe) and cassiterite[J]. *Ore Geology Reviews*, 100: 561-573.
- YAN Q H, WANG H, CHI G X, et al., 2022. Recognition of a 600-km-long Late Triassic rare metal (Li-Rb-Be-Nb-Ta) pegmatite belt in the western Kunlun orogenic belt, Western China[J]. *Economic Geology*, 117(1): 213-236.
- YIN A, HARRISON T M, 2000. Geologic evolution of the Himalayan-Tibetan orogen[J]. *Annual Review of Earth and Planetary Sciences*, 28: 211-280.
- ZHANG X Y, WANG H, YAN Q H, 2022. Garnet geochemical compositions of the Bailongshan lithium polymetallic deposit in Xinjiang Province: implications for magmatic-hydrothermal evolution[J]. *Ore Geology Reviews*, 150: 105178.
- ZHANG Z Y, JIANG Y H, NIU H C, et al., 2021. Fluid inclusion and stable isotope constraints on the source and evolution of ore-forming fluids in the Bailongshan pegmatitic Li-Rb deposit, Xinjiang, western China[J]. *Lithos*, 380-381: 105824.
- ZHENG F B, WANG G G, NI P, 2021. Research progress on the fluid metallogenetic mechanism of granitic pegmatite-type rare metal deposits[J]. *Journal of Geomechanics*, 27(4): 596-613. (in Chinese with English abstract)
- ZHOU Q F, QIN K Z, ZHU L Q, et al., 2023. Overview of magmatic differentiation and anatexis: insights into pegmatite genesis[J]. *Earth Science Frontiers*, 30(5): 26-39. (in Chinese with English abstract)
- ZHOU J S, WANG Q, XU Y G, et al., 2021. Geochronology, petrology, and lithium isotope geochemistry of the Bailongshan granite-pegmatite system, northern Tibet: Implications for the ore-forming potential of pegmatites, *Chemical Geology*, 584: 120484.
- ### 附中文参考文献
- 陈谋, 王核, 张晓宇, 等, 2022. 新疆康西瓦伟晶岩的成矿潜力判断: 来自锆石 U-Pb 年代学、地球化学与 Hf 同位素证据 [J]. *岩石学报*, 38(7): 2095-2112.
- 洪涛, 翟明国, 王岳军, 等, 2023. 锂铍络合物稳定性与花岗伟晶岩中锂铍“差异跃迁”耦合关联 [J]. *地学前缘*, 30(5): 93-105.
- 李建康, 李鹏, 陈振宇, 2023. 锂铍等战略性金属矿产资源成矿规律与预测评价: 前言 [J]. *岩石学报*, 39(7): 1881-1886.
- 李永, 王威, 杜晓飞, 等, 2022. 西昆仑 509 道班西锂铍稀有金属矿白云母<sup>40</sup>Ar/<sup>39</sup>Ar 定年及对区域成矿的限定 [J]. *中国地质*, 49(6): 2031-2033.
- 谭克彬, 郭岐明, 郭勇明, 2021. 新疆和田 509 道班西锂铍多金属矿床花岗岩 U-Pb 年龄及其构造意义 [J]. *新疆有色金属*, 44(2): 6-10.
- 唐俊林, 柯强, 徐兴旺, 等, 2022. 西昆仑大红柳滩地区龙门山锂铍伟晶岩区岩浆演化与成矿作用 [J]. *岩石学报*, 38(3): 655-675.
- 唐文春, 段威, 邹林, 等, 2022. 川西可尔因地区伟晶岩型锂矿地球化学指标定位矿体的方法 [J]. *地质力学学报*, 28(5): 765-792.
- 王登红, 代鸿章, 刘善宝, 等, 2022. 中国锂矿十年来勘查实践和理论研究的十个方面新进展新趋势 [J]. *地质力学学报*, 28(5): 743-764.
- 王核, 李沛, 马华东, 等, 2017. 新疆和田县白龙山超大型伟晶岩型锂铷多金属矿床的发现及其意义 [J]. *大地构造与成矿学*, 41(6): 1053-1062.
- 王核, 徐义刚, 闫庆贺, 等, 2021. 新疆白龙山伟晶岩型锂矿床研究进展 [J]. *地质学报*, 95(10): 3085-3098.
- 王核, 黄亮, 马华东, 等, 2023. 西昆仑大红柳滩—白龙山矿集区锂矿成矿特征与成矿规律初探 [J]. *岩石学报*, 39(7): 1931-1949.
- 王威, 杜晓飞, 刘伟, 等, 2022. 西昆仑 509 道班西锂铍稀有金属矿地质特征与成矿时代探讨 [J]. *岩石学报*, 38(7): 1967-1980.
- 魏小鹏, 王核, 张晓宇, 等, 2018. 西昆仑东部晚三叠世高镁闪长岩的成因及其地质意义 [J]. *地球化学*, 47(4): 363-379.
- 许志琴, 朱文斌, 郑碧海, 等, 2023. 川西甲基卡伟晶岩型锂矿的“多层次穹状花岗岩席”控矿新理论: 记“川西甲基卡锂矿科学钻探”创新成果 [J]. *地质学报*, 97(10): 3133-3146.
- 郑范博, 王国光, 倪培, 2021. 花岗伟晶岩型稀有金属矿床流体成矿机制研究进展 [J]. *地质力学学报*, 27(4): 596-613.
- 周起凤, 秦克章, 朱丽群, 等, 2023. 花岗伟晶岩成因探讨: 岩浆分异与深熔 [J]. *地学前缘*, 30(5): 26-39.